E18-2018-58

A. Pahomi [1,2], M. Balasoiu [2,3], Yu. Gorshkova [2],
V. Turchenko [2,4], A. Kuklin [2,5], N. Lizunov [2], D. Aranghel [3]

SMALL-ANGLE X-RAY SCATTERING OF ALGINATE MEMBRANES DOPED WITH $CoFe_2O_4$ NANOPARTICLES. PRELIMINARY RESULTS

Presented at the International Conference “Biomembranes”, 1–5 October 2018, Dolgoprudny, Russia

---

[1] West University of Timişoara, Timişoara, Romania
[2] Joint Institute for Nuclear Research, Dubna
[3] Horia Hulubei National Institute of Physics and Nuclear Engineering, Bucharest-Magurele, Romania
[4] Donetsk Institute for Physics and Engineering named after O. O. Galkin of the NASU, Kyiv
[5] Moscow Institute of Physics and Technology, Dolgoprudny, Russia

Пахоми А. и др. E18-2018-58

Малоугловое рассеяние рентгеновских лучей на мембранах из альгината, легированных наночастицами $CoFe_2O_4$. Предварительные результаты

Альгинат — биополимер, который наиболее часто используется в сельском хозяйстве, пищевой промышленности и науках о жизни благодаря таким его высокоэффективным свойствам, как гелеобразование и вязкость. Если ранее альгинаты применялись в качестве адгезивных связующих, то в последнее время они широко используются в качестве загустителей, эмульгаторов, пленочных и гелеобразующих веществ. Область применения альгината и магнитных наночастиц может быть расширена на биомедицину и биотехнологии, включая целенаправленную доставку лекарств, отделение магнитных клеток, иммобилизацию ферментов, магнитно-резонансную томографию (МРТ) и лечение гипертермией.

В работе представлены структурные исследования мембран из альгината, легированных наночастицами $CoFe_2O_4$, и их сшивание с $CaCl_2 \cdot 2H_2O$ с помощью методов силовой микроскопии (AFM), сканирующей электронной микроскопии (SEM), рентгеновской дифракции (XRD) и малоуглового рассеяния рентгеновского излучения (SAXS).

Работа выполнена в Лаборатории нейтронной физики им. И. М. Франка ОИЯИ.

Препринт Объединенного института ядерных исследований. Дубна, 2018

Pahomi A. et al. E18-2018-58

Small-Angle X-Ray Scattering of Alginate Membranes Doped with $CoFe_2O_4$ Nanoparticles. Preliminary Results

Today, alginate is one of the most employed biopolymers in agricultural, food and life science related industry, mostly due to its high-performance gelling and viscosity properties. The initial industrial uses of alginates were as adhesive binders, however more recently they are extensively applied as thickeners, emulsifiers, film and gel making substances. The complementary use of alginate and magnetic nanoparticles can lead to new biomedical and biotechnological applications, including targeted drug delivery, magnetic cell separation, enzyme immobilization, magnetic resonance imaging (MRI), and hyperthermia treatments.

In this study, the structural investigations of alginate membranes doped with $CoFe_2O_4$ nanoparticles and the effect of their cross-linking with $CaCl_2 \cdot 2H_2O$ using atomic force microscopy (AFM), scanning electron microscopy (SEM), X-ray diffraction (XRD), and small-angle X-ray scattering (SAXS) methods are presented.

The investigation has been performed at the Frank Laboratory of Neutron Physics, JINR.

Preprint of the Joint Institute for Nuclear Research. Dubna, 2018

INTRODUCTION

Alginates are linear water-soluble polysaccharides comprising (1-4)-linked units of α-D-mannuronate (M) and β-L-guluronate (G) at different proportions and different distributions in the chain [1, 2].

They are present in brown algae and can also be found in metabolic products of some bacteria [3]. The chemical composition and sequence of the M and G residues depend on the biological source and the state of maturation of the plant [4]. The alginates, as well as all the polysaccharides, are polydisperse in terms of molecular mass so that they are more similar to the synthetic polymers than to other biopolymers such as proteins and nucleic acids [5, 6].

Alginates are well-known natural ionic polysaccharides used mainly as food additives, thickeners, gelling agents, and in the controlled delivery of drugs [7–9]. In Fig. 1, the structure of sodium alginate is shown.

A magnetic colloid, also known as a ferrofluid (FF), is a colloidal suspension of single-domain magnetic particles, with typical dimensions of about 10 nm, dispersed in a liquid carrier [11].

In order to avoid agglomeration, the magnetic particles have to be coated with a shell of an appropriate material. According to the coating, the FFs are classified into two main groups: surfacted (SFF), if the coating is a surfactant

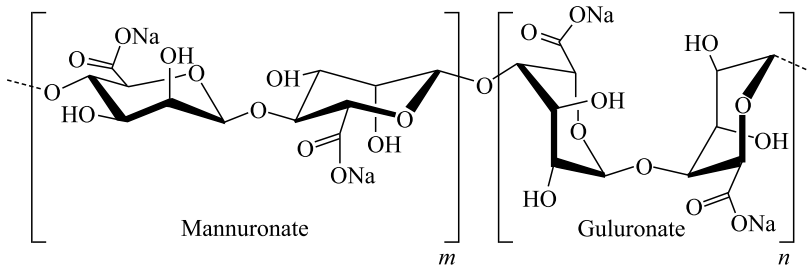

Fig. 1. Representation of the structure of sodium alginate [10]

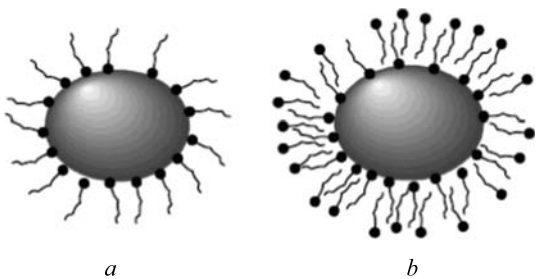

Fig. 2. Sketch of surfacted magnetic particles: *a*) single-layered surfacted nanoparticles; *b*) double-layered surfacted nanoparticles [11]

molecule [11, 12], and ionic (IFF), if it is an electric shell [13]. Figure 2 gives the sketch of surfacted magnetic particles.

Cobalt ferrite nanoparticles ($CoFe_2O_4$) have received increasing attention due to combination of their bulk magnetic properties with the magnetic properties typical of nanoparticles (superparamagnetism) that make them ideal materials for technological and medical applications [14].

By combining the polymer with the nanoparticles in different forms, benefit can be obtained from the combination of the features inherent to both the components, and the new material can have a wide range of applications.

1. EXPERIMENTAL SECTION

1.1. Materials and Membrane Preparation. For this study, we used alginic acid sodium salt with low viscosity and $CoFe_2O_4$ nanoparticles. Alginic sodium salt was purchased from Alpha Aesar, A Johnson Mathey Company; it has the viscosity of 40–90 mPa · s (1% solution) and the pH of 5.0–7.5 (1% solution).

The ferrofluid was prepared at the Institute of Technical Chemistry (Perm, Russia) by the coprecipitation of $Fe(OH)_3$ and $Co(OH)_2$, ferritisation of hydroxide mixture in 1 M alkali aqueous solution, adsorption of lauric acid on ferrite particles, and peptisation of hydrophobic precipitate in aqueous solution with sodium n-dodecyl sulphate [14].

The membranes were prepared by casting from aqueous solutions using the method described by Russo [15]. Two solutions of 1% (wt/v) sodium alginate were prepared, while stirring, at the room temperature for 24 h. After a clear solution was obtained, we added 1 mL of $CoFe_2O_4$/lauric acid/DDS-Na/H_2O ferrofluid in one of the solutions and sonicated it to ensure homogeneous distribution of the nanoparticles in the solution.

The solutions were poured into a glass Petri dish, avoiding bubble formation, and kept in an oven at $50°C$ to ensure the evaporation of the solvent. After the solvent was evaporated, the membranes were peeled off and kept in an exicator till use.

The cross-linking was made with a 3% $CaCl_2 \cdot 2H_2O$ solution in which the membranes were immersed for 30 min, after that they were dried.

Depending on the technique used, sample preparation might be different and it was presented in the Method section.

1.2. Methods of Characterization. *1.2.1. Small-Angle X-Ray Scattering.* Small-angle X-ray scattering (SAXS) is a small-angle scattering (SAS) technique where the elastic scattering of X-rays by a sample, which has inhomogeneities in the nanometer range, is recorded at very low angles (typically $0.1-10°$). This angular range contains information about the shape and size of macromolecules, characteristic distances of partially ordered materials, pore sizes, and other data. SAXS is capable of delivering structural information of macromolecules between 5 and 25 nm, of repeat distances in partially ordered systems of up to 150 nm [16].

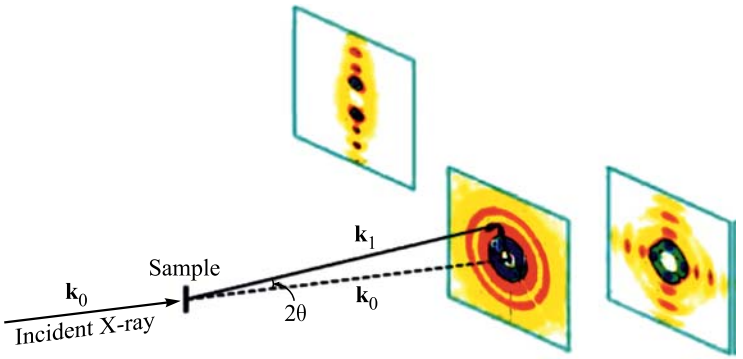

Fig. 3. Principle of SAXS [18]

X-ray scattering techniques are a family of nondestructive analytical techniques which reveal information about the crystallographic structure, chemical composition, and physical properties of materials and thin films [17].

The small-angle X-ray scattering (SAXS) technique (Fig. 3) has been applied to investigate membrane structure of alginate in the absence and presence of divalent cation Ca(II) and $CoFe_2O_4$ nanoparticles.

Sample Preparation. The SAXS measurements were taken with a Rigaku small-angle X-ray scattering (SAXS) pinhole camera system (Japan) installed with a Rigaku MicroMax-007 HF X-ray source.

The membranes were cut in $\sim 1\times1$ cm samples and fixed on a one-sided tape. After that they were mounted on the sample holder facing the beam directly. For the precision of measurement, SAXS analysis was made also for the tape without sample.

1.2.2. Atomic Force Microscopy. Atomic force microscopy (AFM), also known as scanning-force microscopy (SFM), is a type of scanning probe microscope technique. It works by running a sharp tip attached to a cantilever and sensor over the surface of a sample and measuring the surface forces between the probe and the sample [19]. As the cantilever runs along the sample surface, it moves up and down due to the surface features and the cantilever deflects accordingly. This deflection is usually quantifed using an optical sensor, with the laser beam being reflected on the back of the cantilever onto the light detector [19]. AFM does not need to operate in vacuum and can operate in ambient air or under liquid; hence, it is increasingly being used to image biological samples as well as nanoparticles [20–22].

Atomic force microscopy is a relatively nondestructive technique as compared to conventional scanning electron microscopy and transmission electron microscopy. It also has an additional advantage of 3-dimensional measurements of the surface structure of polymers [23].

The direct visualization of 3-dimensional images of the polymer surfaces is helpful for understanding the effects of changes in processing conditions. The field of nanocomposite is emerging at a rapid rate. Atomic force microscopy can be useful for the characterization of these nanocomposite materials.

The conventional surface characterization techniques provide only pictorial images of the polymer surface [24]. Atomic force microscopy can be exploited to measure the mechanical properties, adhesion forces and structure of the polymer surface by making slight changes in the instrumentation involved. The capability of AFM to delineate the phase transitions of polymers provides us with important insight regarding the factors that are responsible for the peculiar properties exhibited by polymers. Thus, complete characterization of a polymer surface is possible by AFM [25].

Sample Preparation. Atomic force microscopy INTEGRA PRIMA was provided by the company NT-MDT Spectrum Instruments (Zelenograd, Russia). AFM images were recorded at semi-contact mode, known as *tapping mode*, with a standard NSG01 and NSG01_Au tips of 10 nm curvature radius (NT-MDT Spectrum Instruments, Zelenograd, Russia) at room temperature. The imaging rate was 0.3 Hz. Both height and phase images were recorded.

AFM imaging was performed on films prepared from alginate solution and alginate solution doped with $CoFe_2O_4$ nanoparticles. Samples were cast as films for ease of imaging. One drop of alginate solution at a given concentration was deposited onto a quartz glass slide, after which the drop was aspirated using a Pasteur pipette and let to dry at room temperature. Calcium chloride at a given concentration was added to the film in a drop-wise fashion to induce cross-linking.

1.2.3. Scanning Electron Microscopy. Scanning electron microscopy (SEM) is useful for detailed study of a specimen's surface. A high-energy electron beam scans across the surface of a specimen, usually coated with a thin film of gold or platinum to improve contrast and the signal-to-noise ratio [26].

As the beam scans across the sample's surface, interactions between the sample and the electron beam result in different types of electron signals emitted at or near the specimen surface [27, 28].

These electronic signals are collected, processed, and eventually translated as pixels on a monitor to form an image of the specimen's surface topography that appears three-dimensional [29].

Sample Preparation. The surface of the samples used in this study was analyzed by a Hitachi SU8020 (Japan) scanning electron microscope at an accelerated voltage of 2 kV. Prior to observation, the samples were coated with a thin layer of gold under vacuum.

1.2.4. X-Ray Diffraction. X-ray diffraction (XRD) is one of the most important nondestructive tools to analyze all kinds of matter. The technique is used for the identification of crystalline phases of various materials and the quantitative phase analysis subsequent to the identification [30].

X-ray diffraction techniques are superior in elucidating the three-dimensional atomic structure of crystalline solids. The properties and functions of materials largely depend on the crystal structures. X-ray diffraction techniques have, therefore, been widely used as an indispensable means in materials research, development and production [31].

Sample Preparation. The presence of the $CoFe_2O_4$ nanoparticles in the membrane was characterized by the XRD technique using X-ray diffractometer (PANalytical Empyrean) with Cu Kα radiation ($\lambda = 0.15406$ nm) in a wide range of $2\theta\,(5^\circ < 2\theta < 80^\circ)$.

The samples were prepared in a similar manner to the ones from atomic force microscopy. Instead of using quartz glass slide, the sample was casted on a zero diffraction plate made of silicon cut at special orientation.

2. RESULTS AND DISCUSSION

2.1. Surface Morphology. As previously stated, AFM method was chosen for imaging, as it provides nanometer resolution and three-dimensional surface imaging, requires minimal sample preparation and allows imaging in ambient and liquid conditions.

It can be seen from the surface imaging (Fig. 4) that the addition of $CoFe_2O_4$ nanoparticles increases the inhomogeneity on the surface of the membranes and aggregates of alginate tend to be formed.

Based on the roughness parameters of 1% alginate membrane (Sq = 5.74 nm and Sa = 3.41 nm) and 1% alginate membrane with nanoparticles (Sq = 44.58 nm and Sa = 32.09 nm), from AFM imaging at a higher resolution, one can see that by adding the nanoparticles the surface roughness increases and bigger pores appear

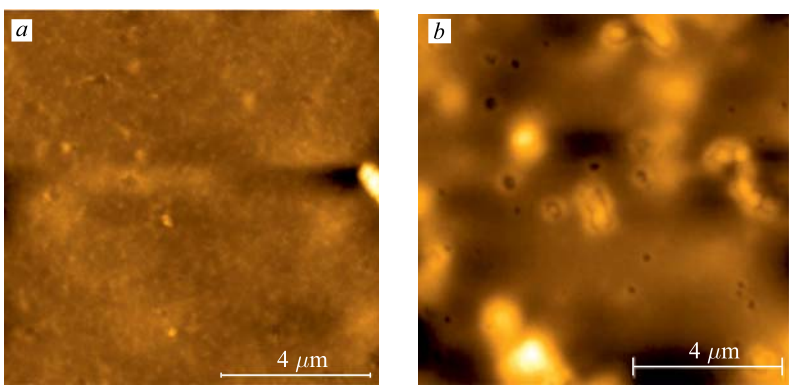

Fig. 4. AFM images of alginate membranes at 10 μm: *a*) 1% sodium alginate; *b*) 1% alginate with $CoFe_2O_4$ nanoparticles

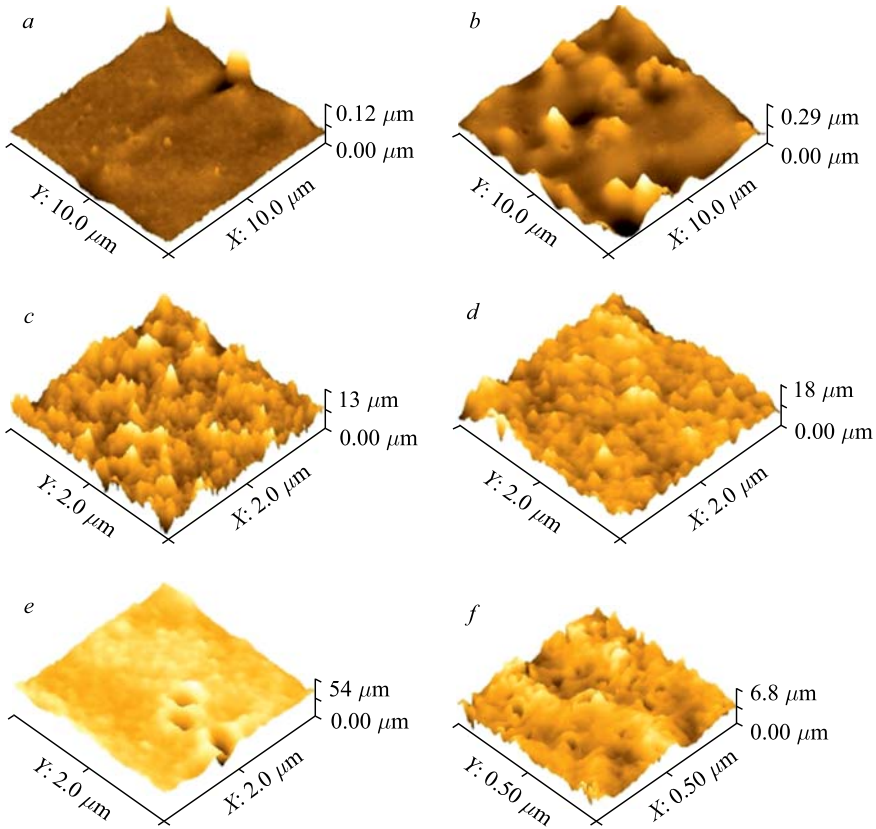

Fig. 5. AFM 3D view of the membranes surface: *a*) 1% alginate membrane (scanning area — 10 μm^2); *b*) 1% alginate membrane with nanoparticles (10 μm^2); *c*) 1% alginate membrane (2 μm^2); *d*) 1% alginate membrane with nanoparticles (2 μm^2); *e*) 1% alginate membrane with nanoparticles and visible pores (2 μm^2); *f*) 1% alginate membrane with nanoparticles (0.5 μm^2)

on the surface. The pore size observed on the membrane with nanoparticles has an average value of 30 nm. Figure 5 shows the 3D AFM images at a higher resolution in which the pores can be observed.

The data obtained from SEM is in accordance with the observation made from AFM imaging. It can be seen in the SEM images of the 1% alginate membrane, without and with nanoparticles, that the surface changes morphology (see Fig. 6). By adding nanoparticles, on the surface of the membrane aggregates with a mean diameter of 50 nm are formed, and one can observe that the nanoparticles are heterogeneously spread on the surface in “pond”-like formations.

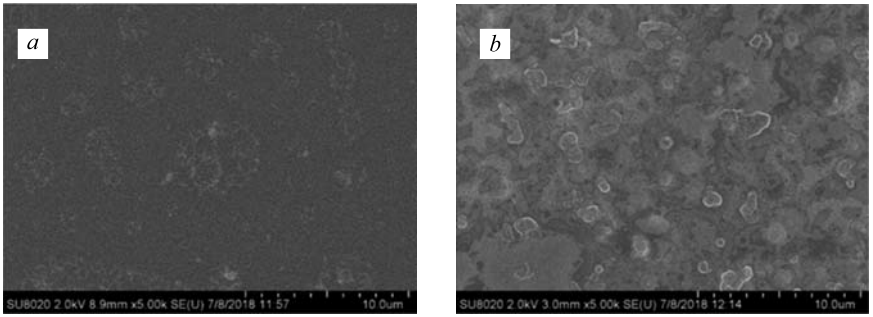

Fig. 6. SEM images of the surface of membranes: *a*) 1% alginate membrane; *b*) 1% alginate membrane with nanoparticles

The aggregates observed in Fig. 6, *b* could be caused by the cross-linking effect of the divalent and trivalent cations present in the nanoparticles formulation (Co^{2+} and Fe^{3+}). It is known that divalent and trivalent cations cross-link the polymeric chains of alginate and rearrange their structure according to the egg-box model (Fig. 7).

The effect of cross-linking with Ca^{2+} ions can be seen in the height images from AFM (Fig. 8) and SEM images (Fig. 9).

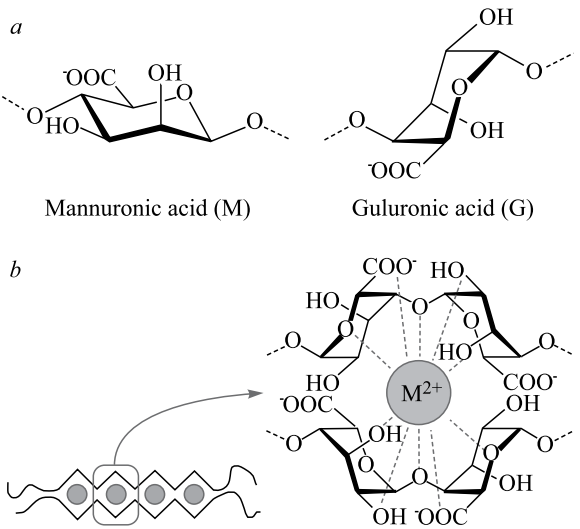

Fig. 7. *a*) Structure of the alginate monomers: D-mannuronic acid (left) and L-guluronic acid (right). *b*) Egg-box structure of the cross-linking between a divalent cation and G monomers of two different alginate chains [32]

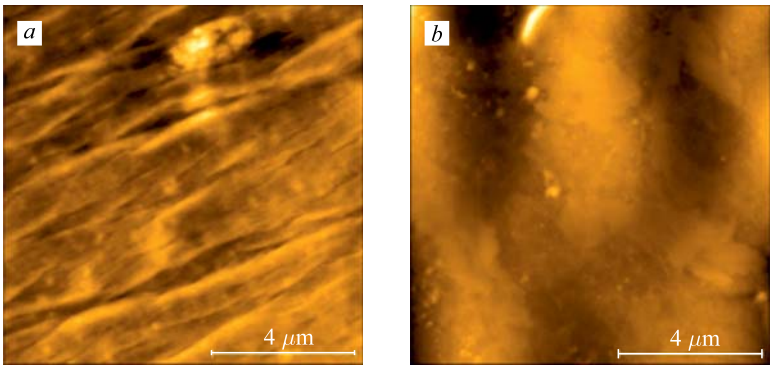

Fig. 8. AFM height image of 1% sodium alginate membrane cross-linked with Ca^{2+} (*a*) and 1% sodium alginate membrane and nanoparticles cross-linked with Ca^{2+} (*b*)

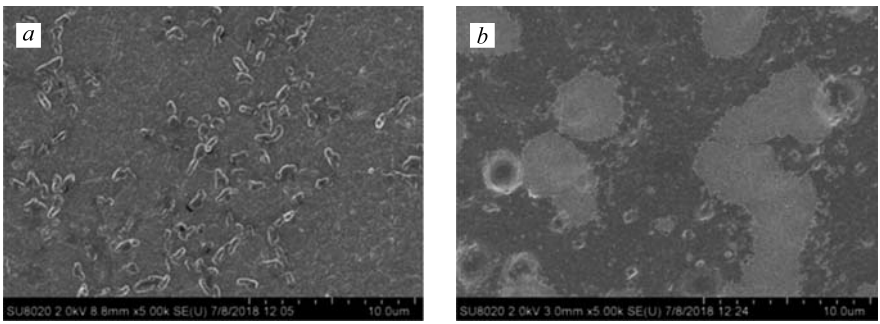

Fig. 9. SEM image of the cross-linked membranes with Ca^{2+}: without nanoparticles (*a*) and with nanoparticles (*b*)

From the AFM image of the sodium alginate membrane cross-linked with Ca^{2+} ions (Fig. 8, *a*) a layered arrangement of the polymer can be observed, which is not found at the cross-linked membranes that have nanoparticles. Also, the roughness parameters of the cross-linked membrane increased (Sq = 29.55 nm and Sa = 22.55 nm), and for the membrane with nanoparticles they decreased (Sq = 27.46 nm and Sa = 21.66 nm).

In the case of divalent cations, egg-box model has illustrated that the cations bond with the blocks of alginate polymers in a planar two-dimensional manner, and the extent of binding increases with an increasing of ionic radius. On the other hand, trivalent cations are expected to form a three-dimensional valent bonding structure with the alginate (Fig. 10) [33].

The cross-linking process is influenced by the ionic radius of the cation. Cations with larger ion radius (Fe^{3+} — 1.35 Å) can form a tighter structure compared with cations with smaller ion radius (Ca^{2+} — 1.0 Å) because they are

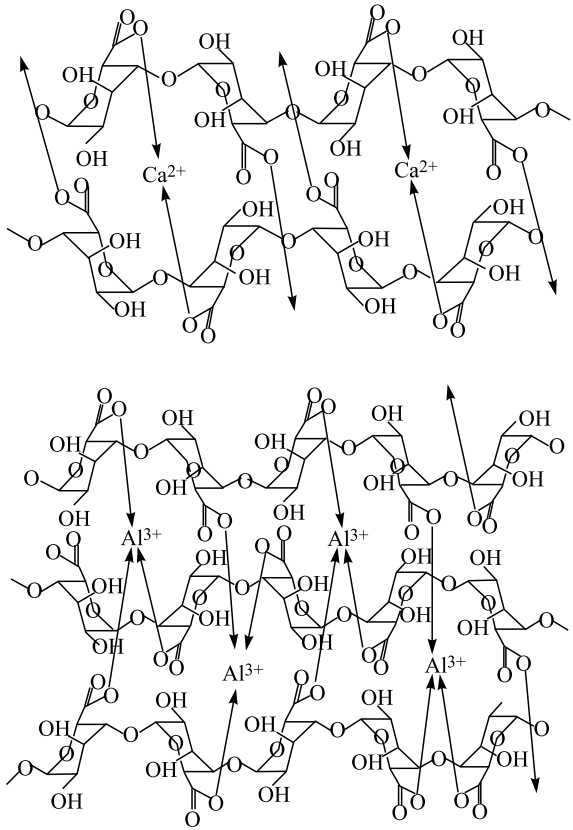

Fig. 10. Example of the mechanism of reaction between calcium and aluminum cations and sodium alginate matrices [33]

expected to fill a larger space between the blocks of alginate polymers, resulting in a tighter arrangement of cross-linked alginate polymers.

Compared with divalent cations, the binding extent of trivalent cations with alginate is enhanced. Trivalent cations could interact with three carboxylic groups of different alginate chains at the same time, lead to a larger coordination number ($(COO)_3M$), and form a three-dimensional valent bonding structure, resulting in a more compact network. These effects were reported in several papers from Al-Musa [33], Yang [34] and Winkleman [35].

As can be seen in Fig. 9, the presence of Fe^{3+} and Co^{2+} in the formulation of the cross-linked membranes compete with the effect of Ca^{2+} cations and the surface from Fig. 9, *b* looks smoother than the one from Fig. 9, *a*.

2.2. SAXS Analysis. The scattering patterns obtained from the SAXS analysis are presented in Fig. 11.

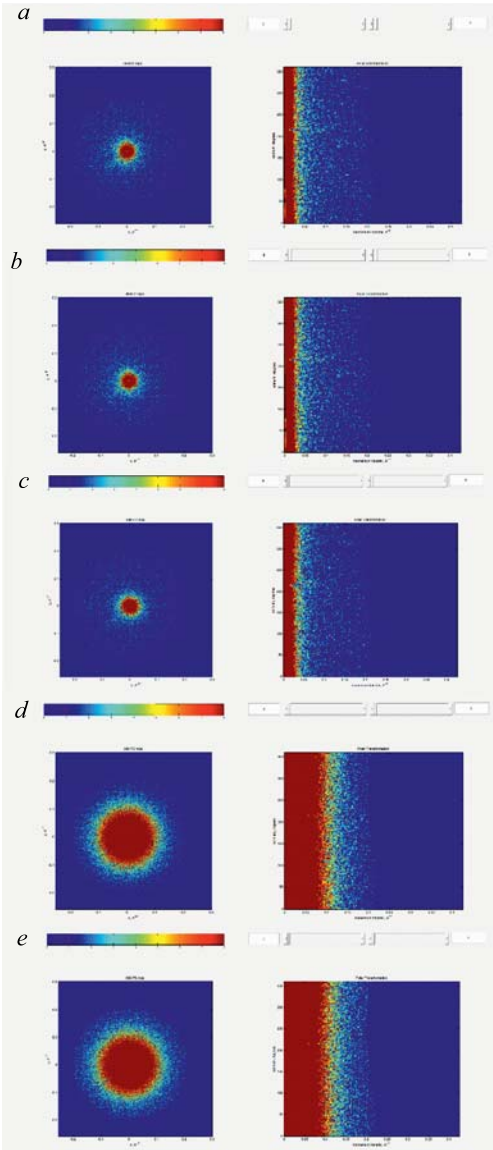

Fig. 11. Scattering patterns of one-sided tape (*a*), 1% sodium alginate membrane (*b*), 1% sodium alginate membrane cross-linked with Ca^{2+} (*c*), 1% sodium alginate membrane and nanoparticles (*d*), 1% sodium alginate membrane and nanoparticles cross-linked with Ca^{2+} (*e*)

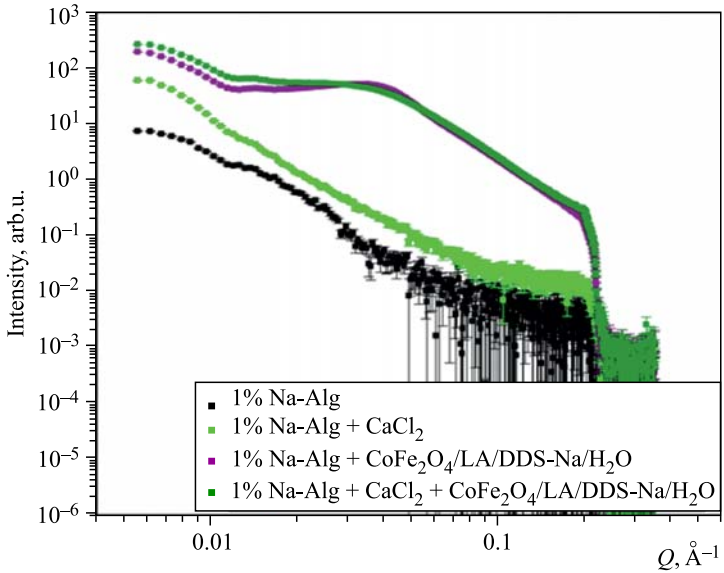

Fig. 12. SAXS curves of the alginate membranes

From the data obtained, the scattering that occurred from the one-sided tape was subtracted and the SAXS data was transformed from 2D to 1D, the following curves being obtained (Fig. 12). The curves were analyzed using Fitter, a program developed by LIT and FLNP (YuMO group), JINR, Dubna.

The fitting models were analyzed on different Q (Å^{-1}) intervals, and the models identified are presented in the table.

2.3. XRD Analysis. Figure 13 shows the XRD patterns of neat alginate powder, 1% sodium alginate membrane and cross-linked membrane with Ca^{2+} cations. Alginate powder exhibited two broad peaks with central positions at $2\theta = 15.7$ and $24.9°$, respectively, which indicate two different amorphous regions. But these two broad peaks do not correlate with the data reported in literature [36–38], where it is stated that alginate exhibits two broad peaks with central positions at $2\theta = 13$ and $21°$.

It can be noticed that for the alginate film, the peak at $24.9°$ is sharper than for the neat alginate powder due to the likely rearrangement of the alginate chains. Such phenomenon was also observed in plasticized chitosan samples obtained by thermo-mechanical mixing [36, 39] and could be an influence of the preparation method, taking into consideration that the membranes were dried at $50°$C. This procedure could have influenced the microstructure of the membranes and there are studies in literature which state that the procedure of drying the membranes can effect the final structure of the product [40–42], so further investigations are required.

Models and scattering parameters obtained from SAXS data using Fitter program

Sample	Q-domain	Model	Scatterer object parameters
1% Na-Alg	0.045–0.11	Ball	Radius — 5306.2 Å
	0.04–0.25	Biaxial ellipsoid	Axis — 865.7 Å Excentricity — 0.9
1% Na-Alg + $CaCl_2$	0.0044–0.023	Prism with edges A, B, C	$A = 7306.8$ Å $B = 7928.1$ Å $C = 7956.3$ Å
	0.03–0.05	Biaxial ellipsoid	Axis — 0.5927 Å Excentricity — 5078
	0.05–0.1	Triaxial ellipsoid with semiaxes a, b, c	$a = 2092.2$ Å $b = 6351.5$ Å $c = 1065.9$ Å
	0.1–0.18	Biaxial ellipsoid	Axis — 30.8 Å Excentricity — 9631
	0.18–0.24	Biaxial ellipsoid	Axis — 62.7 Å Excentricity — 9647
1% Na-Alg + nanoparticles	0.0045–0.0115	Ball	Radius — 5298.3 Å
	0.0115–0.023	Triaxial ellipsoidal coreshell with semiaxes of core a, b, c and thickness of shell t	Semiaxis a of core — 869.5 Å Semiaxis b of core — 19.85 Å Semiaxis c of core — 18.5 Å $t = 6500.3$ Å
	0.02–0.037	Triaxial ellipsoidal coreshell with semiaxes a, b, c and thickness of shell t	Semiaxis a of core — 152.5 Å Semiaxis b of core — 138.7 Å Semiaxis c of core — 137.8 Å $t = 6903.5$ Å
	0.038–0.084	Ball	Radius — 5344.3 Å
1% Na-Alg + nanoparticles + $CaCl_2$	0.006–0.0115	Biaxial ellipsoid	Axis — 191.5 Å Excentricity — 220
	0.0115–0.03	Ball	Radius — 5414.0 Å
	0.04–0.095	Biaxial ellipsoid	Axis — 563.3 Å Excentricity — 352

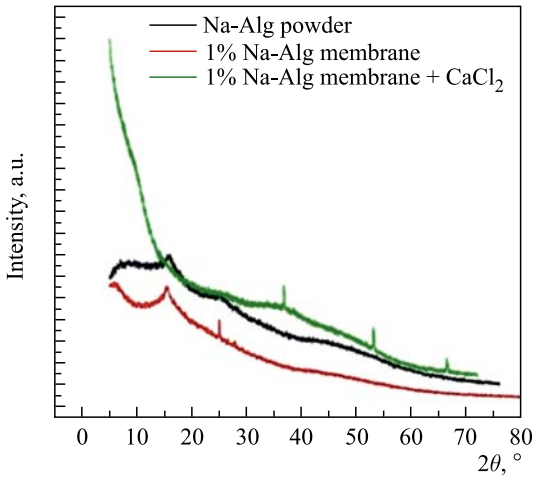

Fig. 13. XRD patterns of neat alginate powder, 1% sodium alginate membrane, and cross-linked membrane with Ca^{2+} cations

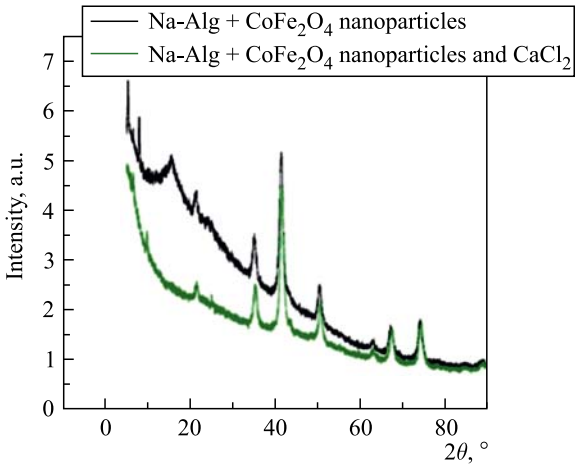

Fig. 14. XRD patterns of 1% sodium alginate membranes with $CoFe_2O_4$ nanoparticles and cross-linked with Ca^{2+} cations

In the XRD spectra of uncross-linked and cross-linked alginate membrane the characteristic peaks disappear, and this could indicate that Na^+ cations are replaced by the Ca^{2+} cations.

In Fig. 14, XRD patterns of alginate membranes with $CoFe_2O_2$ nanoparticles are given. The patterns of both samples show prominent peaks belonging to

the cubic spinel-type lattice of $CoFe_2O_4$, which matches well the standard XRD pattern (JCPDS Card No. 22–1086), and the characteristic peaks from the polymer matrix can be observed.

CONCLUSIONS

The surface morphology of uncross-linked and cross-linked alginate membranes containing $CoFe_2O_4$ nanoparticles was investigated by means of AFM and SEM, and the XRD analysis confirms the $CoFe_2O_4$ nanoparticles presence in the membranes.

AFM experiments performed on alginate membrane containing nanoparticles showed a rough surface and the fact that the presence of nanoparticles promotes the formation of pores.

The presence of Fe^{3+} and Co^{2+} cations in the formulation of the cross-linked membranes competes with the effect of Ca^{2+} cations on the alginate polymer, as can be seen in the AFM and SEM pictures.

Further structural investigations are required to have a better understanding on the factors that can influence the structure of alginate membranes.

Comparing the two-dimensional data obtained from AFM and SEM with the data obtained from the SAXS analysis, we can conclude that the SAXS analysis allowed us to have volume information about the structures present in the membranes:

1. In the SEM image of 1% sodium alginate membrane (Fig. 6, *a*), the ball and ellipsoidal structures can be identified.

2. SAXS allowed us to confirm the observations made about the SEM images (Figs. 6, *b*, and 7) related to the effect of nanoparticles and the cross-linking process with Ca^{2+} cations of the membranes by revealing the complex structures formed, which correspond dimensionally with the ones that appear on the surface of the membranes.

3. The structures identified by SAXS data can be related to the information from literature regarding the effect of divalent and trivalent cations.

Acknowledgements. A. P. is grateful to the organizers of the Summer Student Program for providing education opportunities and valuable experiences. Thanks to E. Karpova and E. Tsukanova for their assistance in solving all the issues and to JINR for the financial support. A. P. expresses special gratitude to Assoc. Prof. V. Chiriac for the given support and incouragement for him to apply for the program and also to the West University of Timisoara which made possible his participation in SSP this summer.

REFERENCES

1. *Grasdalen H., Larsen B., Smisrod O.* ^{13}C-n.m.r. Studies of Monomeric Composition and Sequence in Alginate // Carbohydr. Res. 1981. V. 89, No. 2. P. 179–191.
2. *Wingender J., Neu T. R., Flemming H.-C.* Microbial Extracellular Polymeric Substances: Characterization, Structure and Function. Springer, 1999.

3. *Mushollaeni W., Rusdiana E. S.* Optimizing the Use of Alginate from Sargassum and Padina as Natural Emulsifier and Stabilizer in Cake // J. Agric. Food Technol. 2012. V. 2, No. 7. P. 108–112.
4. *Tønnesen H. H., Karlsen J.* Alginate in Drug Delivery Systems // Drug Dev. Ind. Pharm. 2002. V. 28, No. 6. P. 621–630.
5. *Rinaudo M.* Biomaterials Based on a Natural Polysaccharide: Alginate // Rev. Espec. en Ciencias Quimico-Biologicas. 2014. V. 17, No. 1. P. 92–96.
6. *Gidley M. J., Reid J. S. G.* Galactomannans and Other Cell Wall Storage Polysaccharides in Seeds. Taylor & Francis Group, 2006.
7. *Gombotz W. R., Wee S.* Protein Release from Alginate Matrixes // Adv. Drug Deliv. Rev. 1998. V. 31, No. 3. P. 267–285.
8. *Holte Ø., Onsøyen E., Myrvold R., Karlsen J.* Sustained Release of Water-Soluble Drug from Directly Compressed Alginate Tablets // Eur. J. Pharm. Sci. 2003. V. 20, No. 4–5, P. 403–407.
9. *Liang-Nian H., Robin R. D., Dangsheng S., Pietro T., Conrad Z.* Soil Degradable Bioplastics for a Sustainable Modern Agriculture. Springer US, 2017.
10. *Philippova O., Barabanova A., Molchanov V., Khokhlov A.* Magnetic Polymer Beads: Recent Trends and Developments in Synthetic Design and Applications // Eur. Polym. J. 2011. V. 47, No. 4. P. 542–559.
11. *Raj K., Boulton R. J.* Ferrofluids — Properties and Applications // Mater. Des. 1987. V. 8, No. 4. P. 233–236.
12. *Shokrollahi H.* Structure, Synthetic Methods, Magnetic Properties and Biomedical Applications of Ferrofluids // Mater. Sci. Eng. C. Mater. Biol. Appl. 2013. V. 33, No. 5. P. 2476–2487.
13. *Roger J., Pons J. N., Massart R., Halbreich A., Bacri J. C.* Some Biomedical Applications of Ferrofluids // Eur. Phys. J. Appl. Phys. 1999. V. 5, No. 3. P. 321–325.
14. *Balasoiu M. et al.* Microstructure Investigation of a $CoFe_2O_4$/Lauric Acid/DDS-Na/H_2O Ferrofluid // J. Optoelectronics Adv. Mater. 2015. V. 17, No. 7–8. P. 1114–1121.
15. *Russo R., Malinconico M., Santagata G.* Effect of Cross-Linking with Calcium Ions on the Physical Properties of Alginate Films // Biomacromolecules. 2007. V. 8, No. 10. P. 3193–3197.
16. *Glatter O., Kratky O.* Small Angle X-Ray Scattering. London: Acad. Press, 1982. P. 262.
17. *Gebel G., Diat O.* Neutron and X-Ray Scattering: Suitable Tools for Studying Ionomer Membranes // Fuel Cells. 2005. V. 5, No. 2. P. 261–276.
18. *Fujimura M., Hashimoto T., Hawai H.* Small-Angle X-Ray Scattering Study of Perfluorinated Ionomer Membranes. 1. Origin of Two Scattering Maxima // Macromolecules. 1981. V. 14, No. 5. P. 1309–1315.
19. *Sitterberg J., Özcetin A., Ehrhardt C., Bakowsky U.* Utilising Atomic Force Microscopy for the Characterisation of Nanoscale Drug Delivery Systems // Eur. J. Pharm. Biopharm. 2010. V. 74, No. 1. P. 2–13.

20. *Liang X., Mao G., Ng K. Y. S.* Probing Small Unilamellar EggPC Vesicles on Mica Surface by Atomic Force Microscopy // Colloids Surf. B: Biointerfaces. 2004. V. 34, No. 1. P. 41–51.
21. *Ruozi B., Tosi G., Forni F., Fresta M., Vandelli M. A.* Atomic Force Microscopy and Photon Correlation Spectroscopy: Two Techniques for Rapid Characterization of Liposomes // Eur. J. Pharm. Sci. 2005. V. 25, No. 1. P. 81–89.
22. *Ruozi B. et al.* AFM Phase Imaging of Soft-Hydrated Samples: A Versatile Tool to Complete the Chemical-Physical Study of Liposomes // J. Liposome Res. 2009. V. 19, No. 1. P. 59–67.
23. *Jagtap R. N., Ambre A. H.* Overview Literature on Atomic Force Microscopy (AFM): Basics and Its Important Applications for Polymer Characterization // Indian J. Eng. Mater. Sci. 2006. V. 13. P. 368–384.
24. *Marrese M., Guarino V., Ambrosid L.* Atomic Force Microscopy: A Powerful Tool to Address Scaffold Design in Tissue Engineering // J. Funct. Biomater. 2017. V. 8, No. 1. P. 7.
25. *Raposo M., Ferreira Q., Ribeiro P. A.* A Guide for Atomic Force Microscopy Analysis of Soft-Condensed Matter // Mod. Res. Educ. Top. Microsc. 2007. P. 758–769.
26. *Arzate-Vázquez I. et al.* Microstructural Characterization of Chitosan and Alginate Films by Microscopy Techniques and Texture Image Analysis // Carbohydr. Polym. 2012. V. 87, No. 1. P. 289–299.
27. *Kowalik-Klimczak A., Bednarska A., Gradkowski M.* Scanning Electron Microscopy (SEM) in the Analysis of the Structure of Polymeric Nanofiltration Membranes // Probl. Eksploat. — Maint. Probl. 2016. P. 119–128.
28. *Abdullah S. Z., Bérubé P. R., Horne D. J.* SEM Imaging of Membranes: Importance of Sample Preparation and Imaging Parameters // J. Memb. Sci. 2014. V. 463. P. 113–125.
29. *Kim K. J., Dickson M. R., Fane A. G., Fell J. D.* Electron Microscopy in Synthetic Polymer Membrane Research // J. Microsc. 1991. V. 162, No. 162. P. 403–413.
30. *Podberezskaya N. V., Bragg W. L., Division S.* X-Ray Diffraction Analysis: A Brief History and Achievements // J. Struct. Chem. 2012. V. 53, No. S1. P. 1–3.
31. *Speakman S. A.* Introduction to X-Ray Powder Diffraction Data Analysis // Mater. Sci. 2014. P. 20.
32. *Pistone S., Qoragllu D., Smistad G., Hiorth M.* Formulation and Preparation of Stable Cross-Linked Alginate-Zinc Nanoparticles in the Presence of a Monovalent Salt // Soft Matter. 2015. V. 11, No. 28. P. 5765–5774.
33. *Al-Musa S., Abu Fara D., Badwan A. A.* Evaluation of Parameters Involved in Preparation and Release of Drug Loaded in Crosslinked Matrices of Alginate // J. Control. Release. 1999. V. 57, No. 3. P. 223–232.
34. *Yang C. H. et al.* Strengthening Alginate/Polyacrylamide Hydrogels Using Various Multivalent Cations // ACS Appl. Mater. Interfaces. 2013. V. 5, No. 21. P. 10418–10422.
35. *Winkleman A., Bracher J. P., Gitlin I., Whitesides M. G.* Fabrication and Manipulation of Ionotropic Hydrogels Crosslinked by Paramagnetic Ions // Chem. Mater. 2013. V. 6, No. 8. P. 1362–1368.

36. *Gao C., Pollet E., Avérous L.* Properties of Glycerol-Plasticized Alginate Films Obtained by Thermo-Mechanical Mixing // Food Hydrocoll. 2017. V. 63. P. 414–420.

37. *Atkins E. D. T., Nieduszynski I. A., Mackie W., Parker K. D., Smolko E. E.* Structural Components of Alginic Acid. II. The Crystalline Structure of Poly-α-L-Guluronic Acid. Results of X-Ray Diffraction and Polarized Infrared Studies // Biopolymers. 1973. V. 12, No. 8. P. 1879–1887.

38. *Atkins E. D. T., Nieduszynski I. A., Mackie W., Parker K. D., Smolko E. E.* Structural Components of Alginic Acid. I. The Crystalline Structure of Poly-β-D-Mannuronic Acid. Results of X-Ray Diffraction and Polarized Infrared Studies // Biopolymers. 1973. V. 12, No. 8. P. 1865–1878.

39. *Matet M., Heuzey M. C., Pollet E., Ajji A., Avérous L.* Innovative Thermoplastic Chitosan Obtained by Thermo-Mechanical Mixing with Polyol Plasticizers // Carbohydr. Polym. 2013. V. 95, No. 1. P. 241–251.

40. *Haidara L. H., Vonna L., Vidal L.* Unrevealed Self-Assembly and Crystallization Structures of Na-Alginate, Induced by the Drying Dynamics of Wetting Films of the Aqueous Polymer Solution // Macromolecules. 2010. V. 43, No. 5. P. 2421–2429.

41. *Feng L., Cao Y., Xu D., Wang S., Zhang J.* Molecular Weight Distribution, Rheological Property and Structural Changes of Sodium Alginate Induced by Ultrasound // Ultrason. Sonochem. 2017. V. 34. P. 609–615.

42. *Soazo M. et al.* Heat Treatment of Calcium Alginate Films Obtained by Ultrasonic Atomizing: Physicochemical Characterization // Food Hydrocoll. 2015. V. 51. P. 193–199.

Received on October 31, 2018.

Редактор *Е. И. Крупко*

Подписано в печать 25.12.2018.
Формат 60 × 90/16. Бумага офсетная. Печать офсетная.
Усл. печ. л. 1,25. Уч.-изд. л. 1,60. Тираж 195 экз. Заказ № 59582

Издательский отдел Объединенного института ядерных исследований
141980, г. Дубна, Московская обл., ул. Жолио-Кюри, 6.
E-mail: publish@jinr.ru
www.jinr.ru/publish/